Acquisition of polychromatic data

Charles P. Ursenbach, John C. Bancroft, Malcolm B. Bertram, Henry C. Bland, Eric V. Gallant, Arnim B. Haase, Kevin W. Hall, Don C. Lawton, Gary F. Margrave and Robert R. Stewart

ABSTRACT

In June 2007 CREWES sponsored the acquisition of a polychromatic survey. A vibrator source was used to collect surface seismic data in several narrow frequency ranges, with sources and receivers arranged in a typical 3-D acquisition layout. Data from a 2-D line of receivers show expected features for correlated shot records. Individual uncorrelated traces differ greatly in appearance between narrow-band and broad-band cases.

The broad-band data, correlated and uncorrelated, can be decomposed by bandpass filtering into approximations of narrow-band data. The pseudo-narrow-band correlated shot records are similar in appearance to the true narrow-band shot records, particularly at lower frequencies. In the reverse operation, narrow-band shot records can also be combined to mimic a broad-band shot record. However the narrow frequency bands produce Klauder wavelets with pronounced side lobes, and these persist into the combined result. Using more smoothly defined bands would help to alleviate this shortcoming. Decomposing broad-band uncorrelated traces appears to produce little similarity to narrow-band traces. Expanding the time window of the sweep related to a given frequency range however reveals a degree of similarity.

Multiple sweeps were collected for each source-receiver pair, and displays of repeated sweeps show a high degree of reproducibility.

INTRODUCTION

There are a variety of reasons why it is of interest to explore the acquisition of multiple single-frequency or narrow-band seismic responses. Such a collection we refer to as a *polychromatic survey*, and a proposal for such was presented by CREWES in 2006 (Ursenbach et al., 2006). The primary purpose in acquiring polychromatic data is in connection with the development of *Q*-estimation methods for surface seismic data. Some other potential uses of such data are signal enhancement areas, development of unique time-independent imaging methods, and testing of time-variant spectral methods. These topics are discussed in greater detail in our proposal (Ursenbach et al., 2006).

Here we report on initial efforts to collect polychromatic data. In our proposal, we considered a variety of acquisition modes. One of these, the overlapping narrow frequency bands approach, was employed in this survey.

The objective of this approach is to choose a band which is a small fraction of a typical seismic band, but broad enough to damp out mechanical resonance which might damage the vibrator. Ideally, one would like to employ Gaussian-shaped narrow bands, in which each band is smoothly tapered throughout to form a sweep with a Gaussian

envelope. Such a sweep may provide a Klauder wavelet which is optimally compact in both time and frequency. A set of envelopes would be chosen so that their superposition would result in a function which is nearly constant throughout the cumulative frequency range.

For practical reasons, this initial acquisition employed an approximation consisting of overlapping trapezoidal bands. Further customization of the vibrator software would allow us to employ true Gaussian bands in future. At this stage our goal was to acquire data and assess whether it could be useful for further processing and interpretation projects, or whether data should be reacquired with modified techniques.

ACQUISITION PARAMETERS

Polychromatic data were acquired at the Alder Flats, coalbed methane survey site. For a complete description of the acquisition design, see Lu et al. (2007) in this volume. All of the data in this report are from the northernmost line of receivers located a perpendicular distance 135 m north of a single source location. Other polychromatic data collected (but not shown in this report) include vertical geophone data for the full 3D spread (Sensor SM24, 10 Hz, 0.7 damping), two horizontal components for one line of receivers, and downhole VSP data. The survey employed an ARAM Aries recording system. The vibrator location was a cleared surface with light gravel cover near the injection well of the CBM project.

For each source-receiver pair, a conventional sweep was acquired, as well as several narrow-band sweeps. All sweeps were acquired with 1 ms sample interval. The conventional sweep was a 12 s linear sweep from 10 to 120 Hz, with a 0.5 s taper at each end. The narrow band sweeps were also of 12 seconds' duration, but only swept through a 12 Hz range of frequencies. A 1 s taper was applied at each end, so the frequency content was focused on the central 10 Hz of the range. The narrow-band ranges employed were 14-26 Hz, 24-36 Hz, 34-46 Hz, and so on up to 94-106 Hz.

Four sweeps were recorded for each source-receiver pair and frequency range (both conventional and narrow-band). Uncorrelated data were written to separate SEG-Y files on disk for each sweep. A fifth file containing diversity stacked and correlated data was also stored.

CORRELATED SHOT RECORDS

The correlated shot records for four representative frequency ranges are displayed in Figures 1-4. For comparison we also include idealized Klauder wavelets calculated with the CREWES Matlab toolbox routine 'wavevib' (Margrave, 2007). (Note that this routine was modified to allow an arbitrary taper.) Figure 1 contains the broad-band results (10-120 Hz), Figure 2 contains a low-frequency range (14-26 Hz), Figure 3 contains a mid-frequency range (54-66 Hz), and Figure 4 contains a high-frequency range (94-106 Hz).

Two strong hyperbolae are evident in Figure 1a, with apices at about 80 ms and 380 ms, which represent direct arrivals and air blast. A reflection event is visible at about 300 ms.

The two strong events are visible in each section, with expected frequency content. Also as expected, events in the broad-band section are more temporally localized. For the mid- and high-frequency displays, the side lobe structure of the Klauder wavelet is evident in the shot records, with side-lobe envelopes of ~100 ms duration. The reflection event at 300 ms is obscured in the narrow-band records by side lobes from the strong events.

(a)

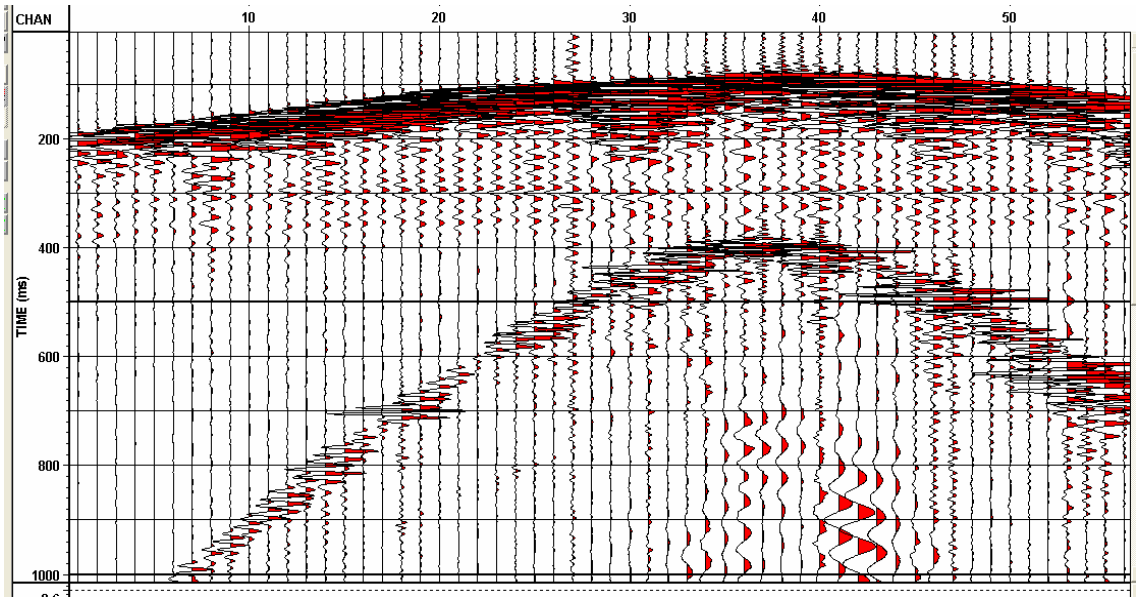

(b)

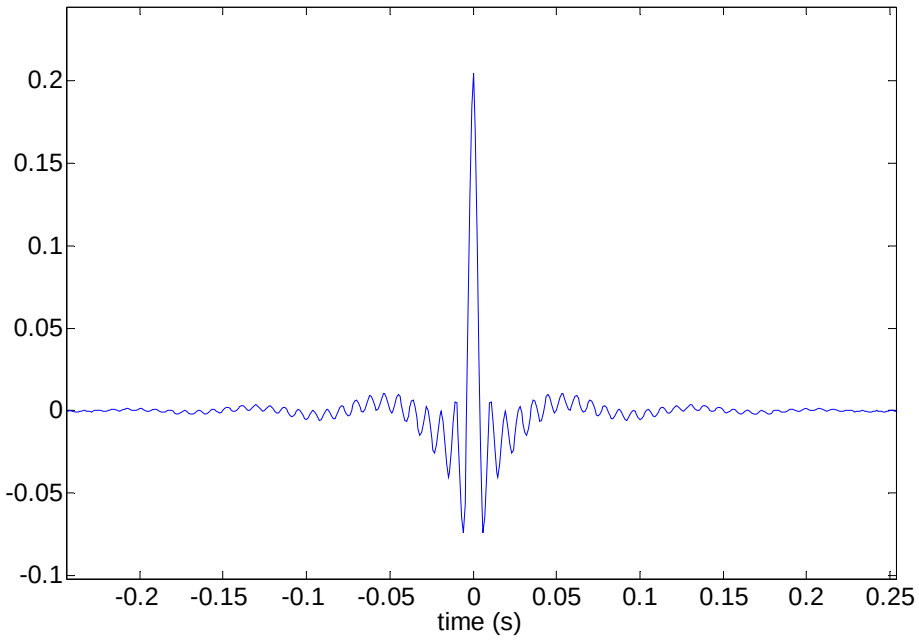

FIG. 1. (a) Broad-band shot record. (b) Corresponding Klauder wavelet. Note the difference in horizontal scale relative to Figures 2b, 3b and 4b.

(a)

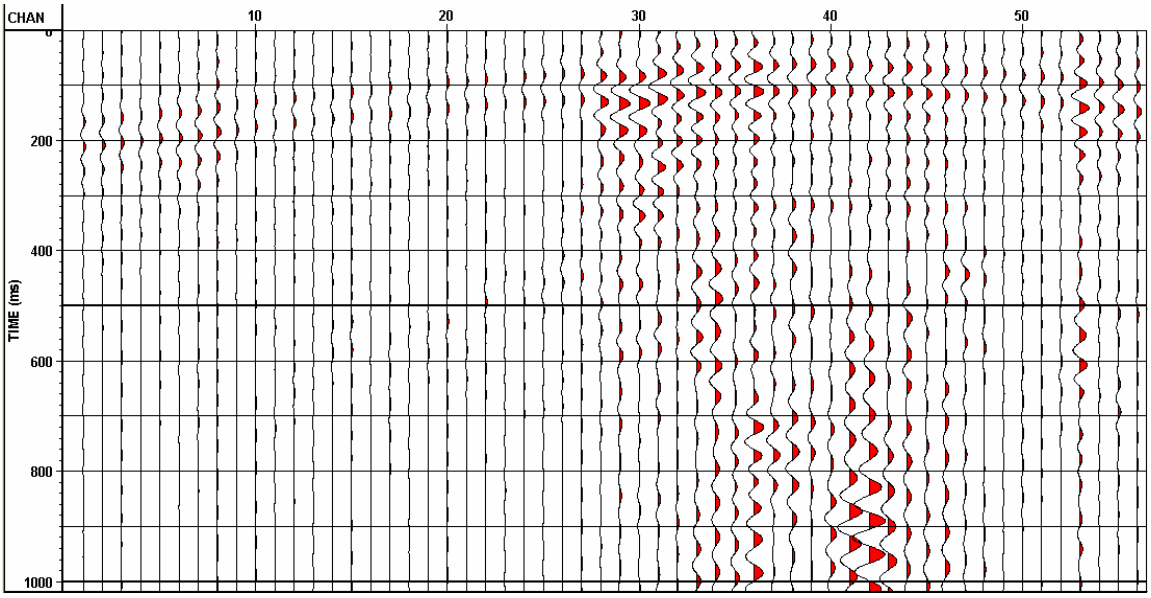

(b)

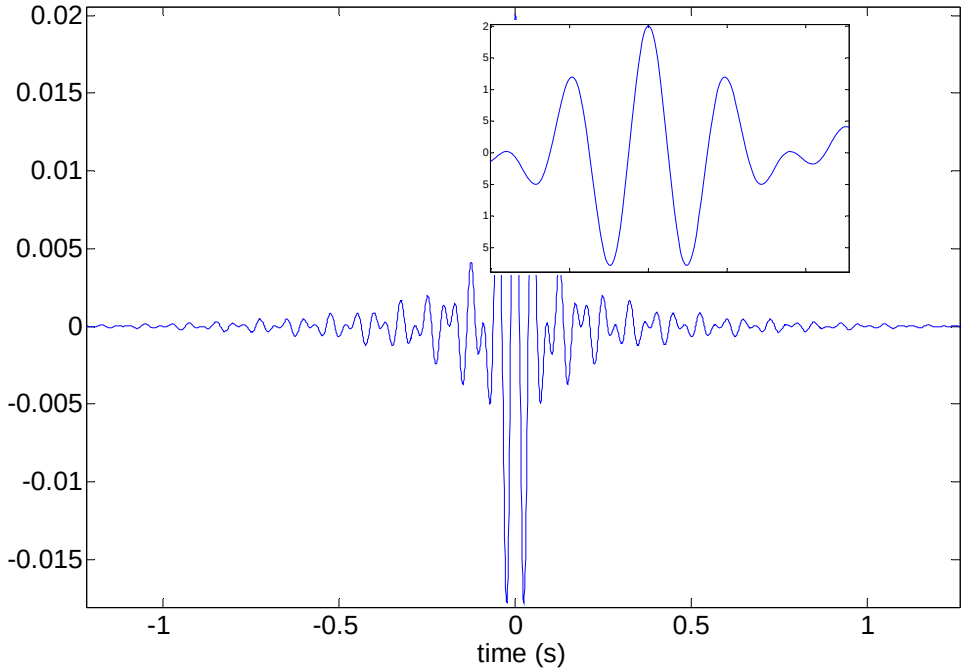

FIG. 2. (a) Low-frequency shot record (14-26 Hz). (b) Corresponding Klauder wavelet. Inset shows detail of central lobe.

(a)

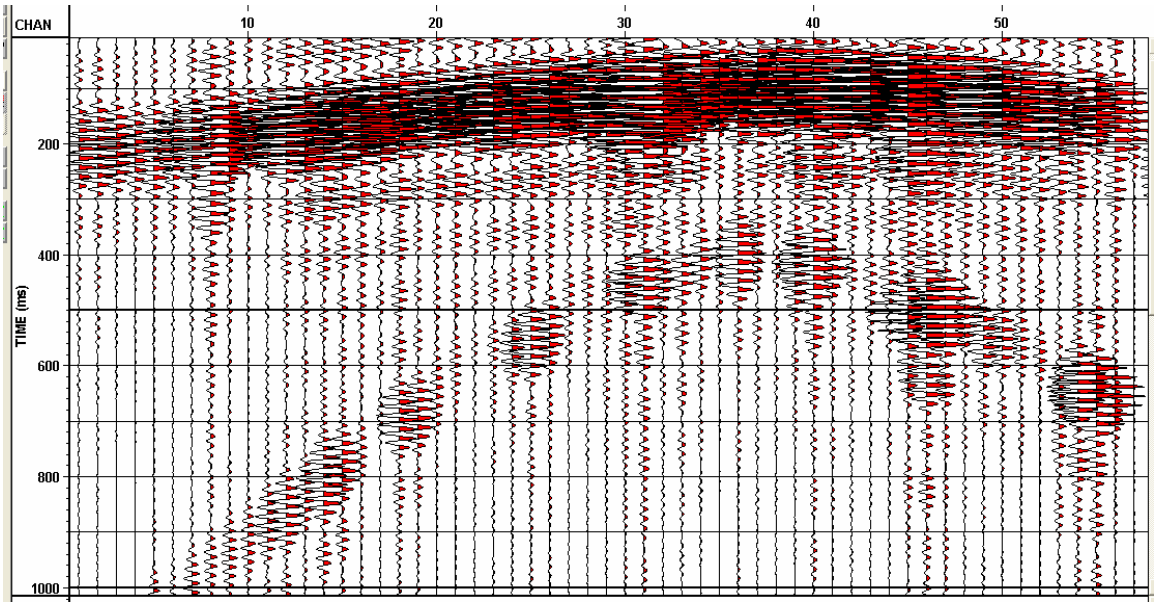

(b)

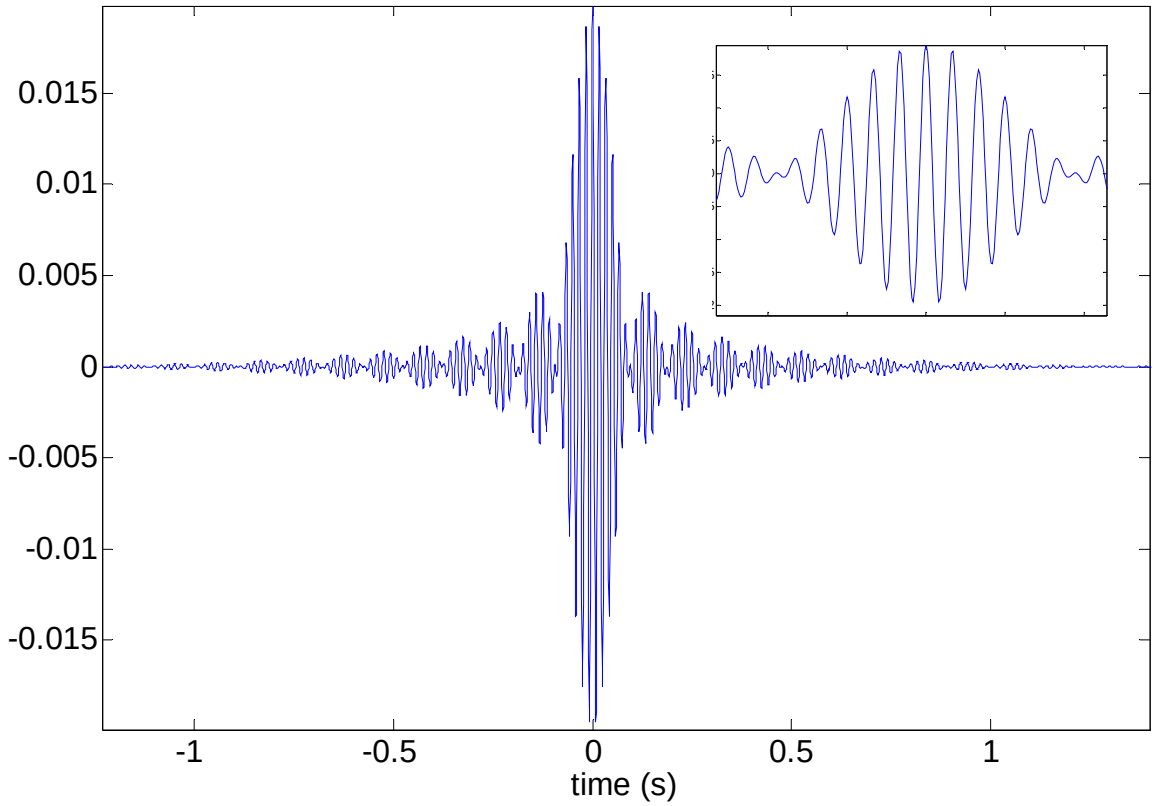

FIG. 3. (a) Mid-frequency shot record (54-66 Hz). (b) Corresponding Klauder wavelet. Inset shows detail of central lobe.

(a)

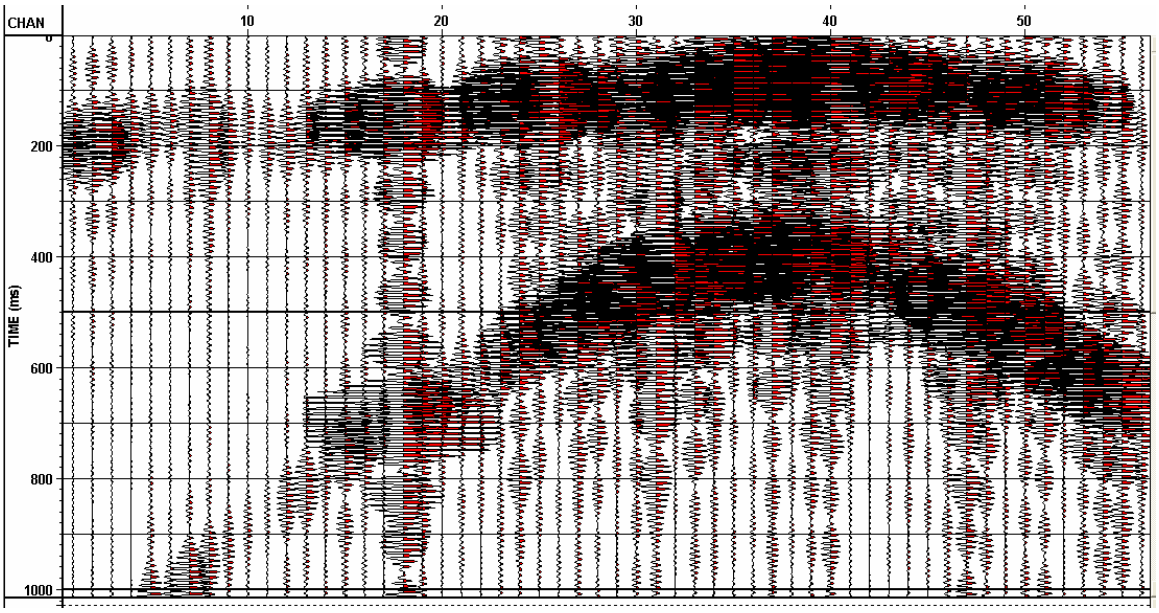

(b)

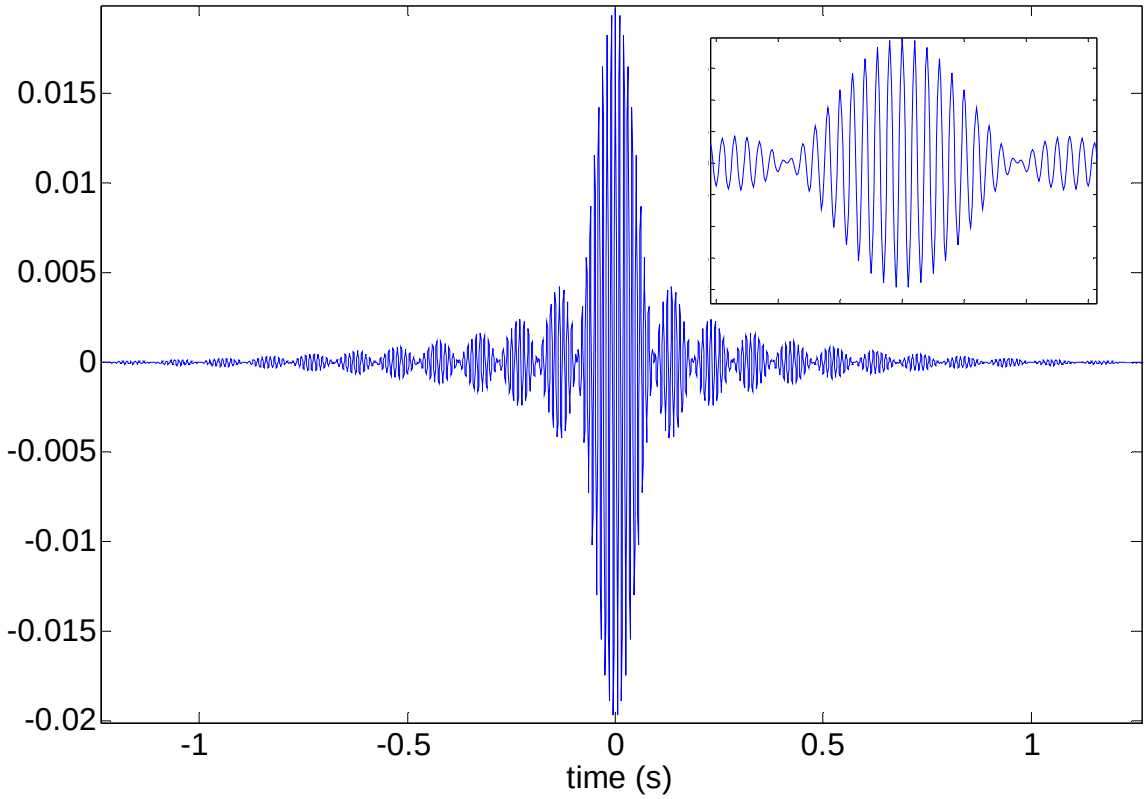

FIG. 4. (a) High-frequency shot record (94-106 Hz). (b) Corresponding Klauder wavelet. Inset shows detail of central lobe.

UNCORRELATED TRACES

Traces of uncorrelated data are shown in Figures 5-8 for the same frequency ranges as in Figures 1-4. Traces 7 to 37 are shown, from the point the two hyperbolae are both visible in Figures 1-4 up to the apex location.

The broad-band and narrow-band traces differ significantly in appearance. Most of the narrow-band traces appear to be contained within periodically varying envelopes, whose overall magnitude varies little over the duration of the trace. The broad-band traces have a more complex shape which increases in overall magnitude up to about 5 or 6 seconds and then decreases exponentially. This is presumably due to the greater attenuation of high-frequencies.

Because the narrow-band sweeps involve such a small range of frequencies, applying a narrow bandpass filter to the uncorrelated traces should remove a considerable amount of out-of-band noise. To demonstrate this, an Ormsby filter is applied which is slightly larger than the narrow bands themselves. For example, a 13/14-26/27 Hz filter is applied to the 14-26 Hz sweep. As shown in Figures 6b, 7b and 8b, the low-frequency traces are affected considerably, the mid-frequency traces very little, and the high-frequency traces moderately.

For comparison we also include idealized sweeps calculated with the CREWES Matlab toolbox routine 'sweep' (Margrave, 2007). Figure 5b displays the broad-band sweep. Because of the denseness of this image, some display aliasing is apparent. In Figures 5c, 6c, 7c and 8c, we show superpositions of sweeps. These were each created by generating a sweep for the appropriate band, and adding it to a time-shifted copy of itself. Each figure shows three such superpositions. In the first, the time-shift is equal to the time separation of the two strong hyperbolae for Trace #7, about 84 ms. In the third the time shift is equal to the separation of the two apices, about 30 ms. In the second, the time shift is midway between these two, 57 ms.

For the mid- and high-frequency traces (Figures 7 and 8) these composite sweeps possess oscillatory envelopes similar to those of the uncorrelated traces. There are about nine lobes for the largest time shift and about three for the smallest time shift. This simple model then appears to adequately explain the envelope structure of these uncorrelated traces. They have been generated with 1 ms sampling, although 0.5 ms sampling was carried out to ensure that envelope oscillations are not due to aliasing.

Even though the broad-band traces possess a more complicated structure, the higher frequency lobe structure of Figure 5c can still be discerned in Figure 5a.

The low-frequency result of Figure 6 does not seem to be explained adequately by the simple sweep model.

(a)

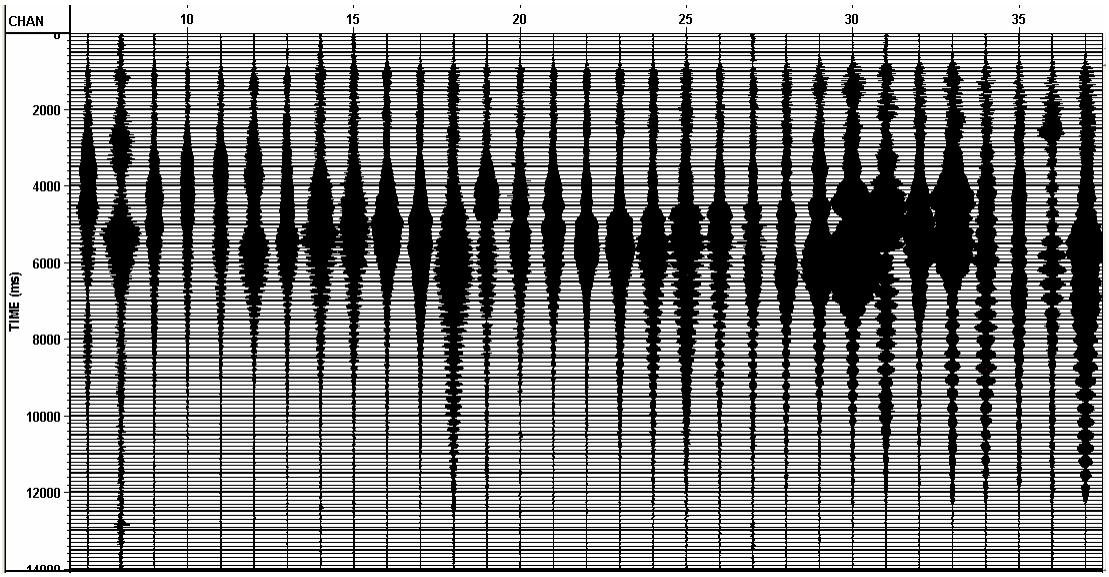
CHAN
10
15
20
25
30
35
TIME (ms)
2000
4000
6000
8000
10000
12000

(b)

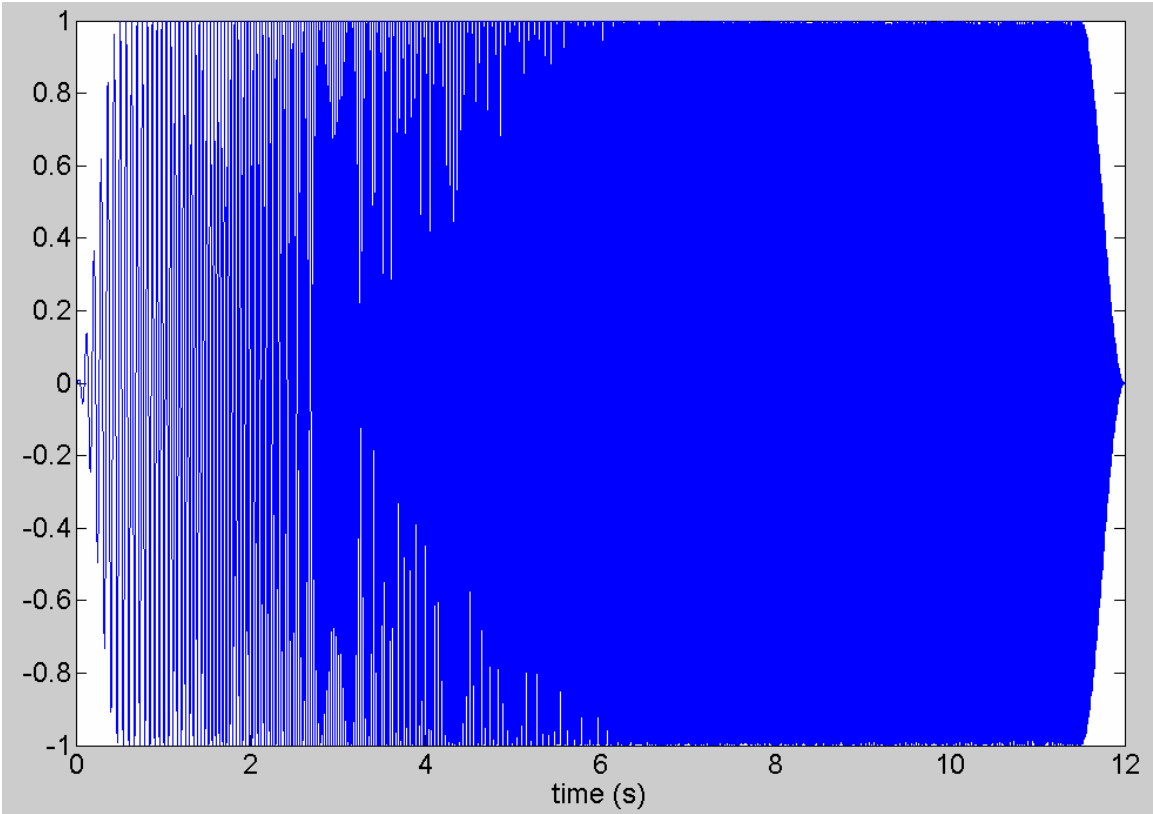
1
0.8
0.6
0.4
0.2
0
-0.2
-0.4
-0.6
-0.8
-1
0
2
4
6
8
10
12
time (s)

(c)

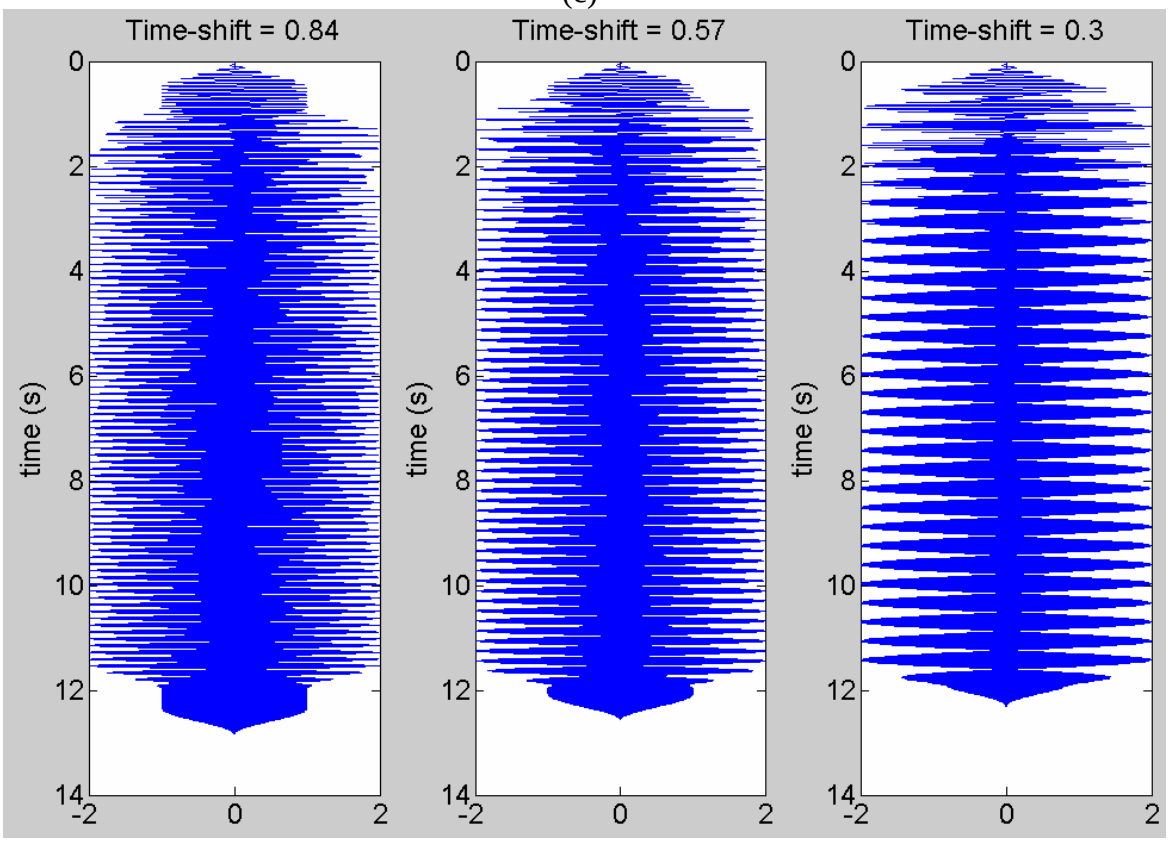

FIG. 5. (a) Broad-band traces. (b) Broad-band sweep. (c) Superpositions of (b) with time-shifted copies of itself. The time shifts correspond to two-way time differences between the two strong hyperbolae in (a), as described in the text.

(a)

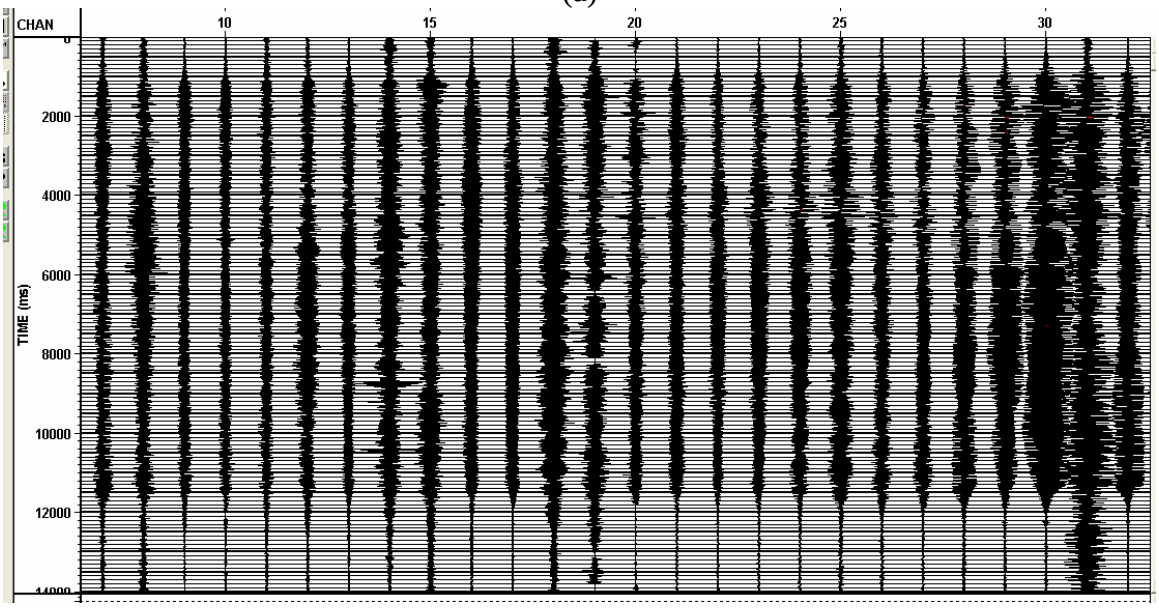

(b)

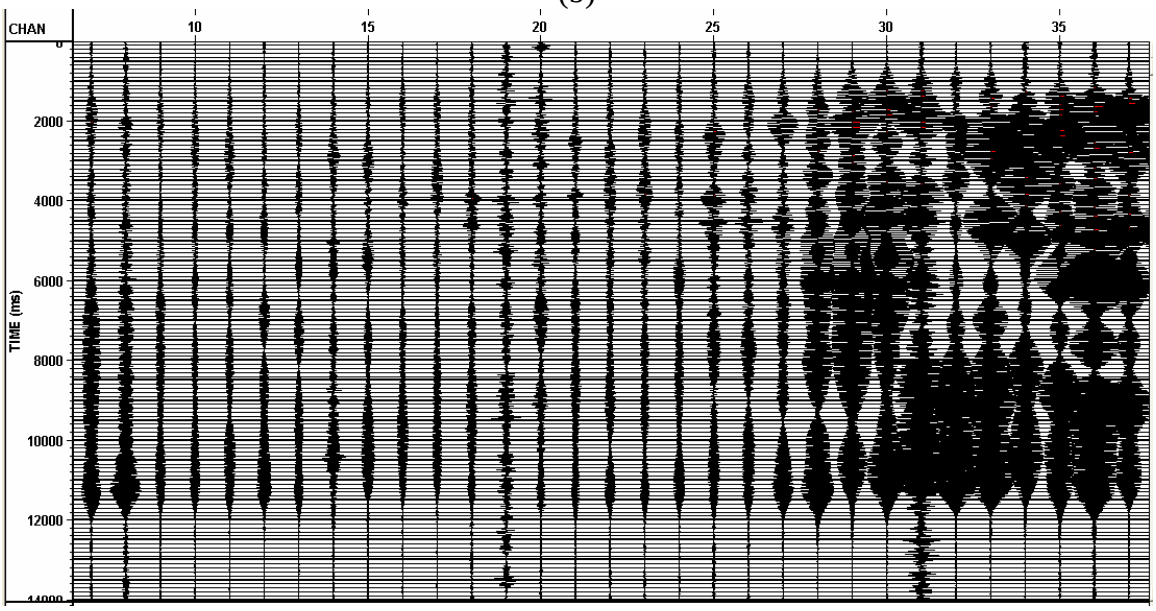

(c)

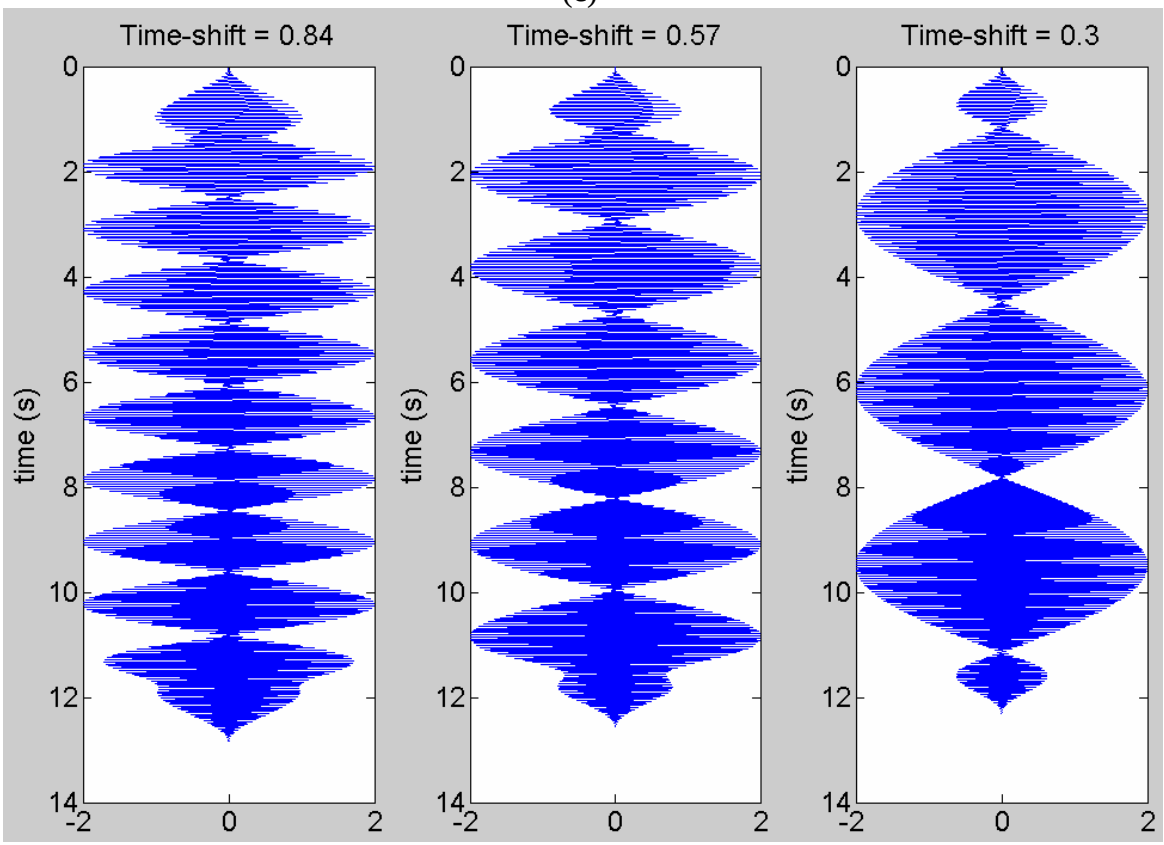

FIG. 6. (a) Low-frequency traces. (b) Filtered low-frequency traces. (c) Superpositions of low-frequency sweep with time-shifted copies of itself.

(a)

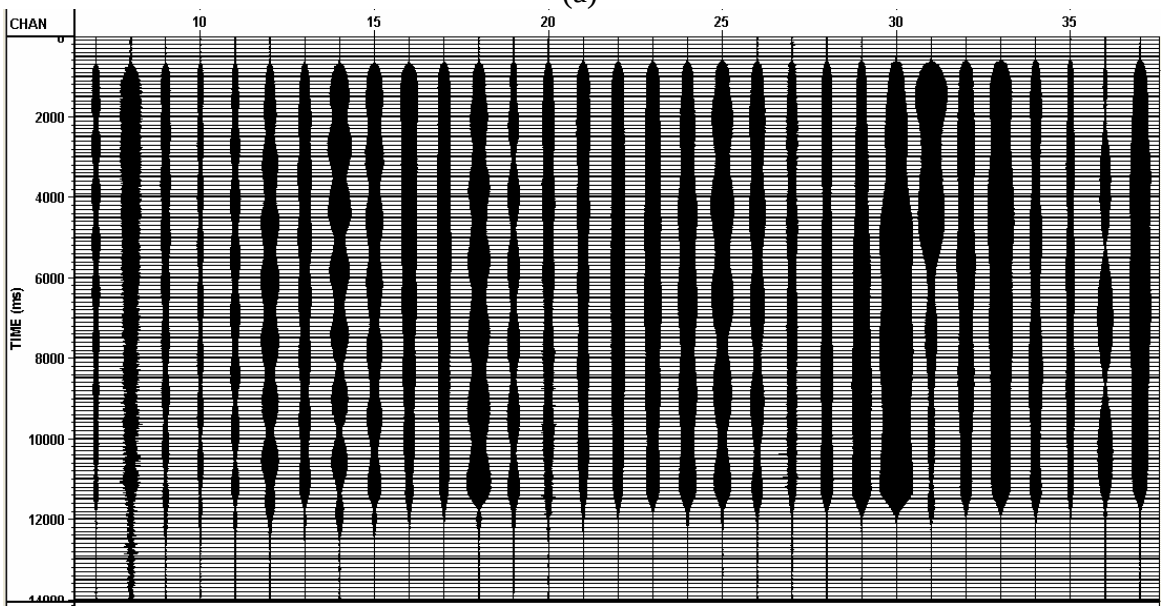
CHAN
10
15
20
25
30
35
TIME (ms)
2000
4000
6000
8000
10000
12000

(b)

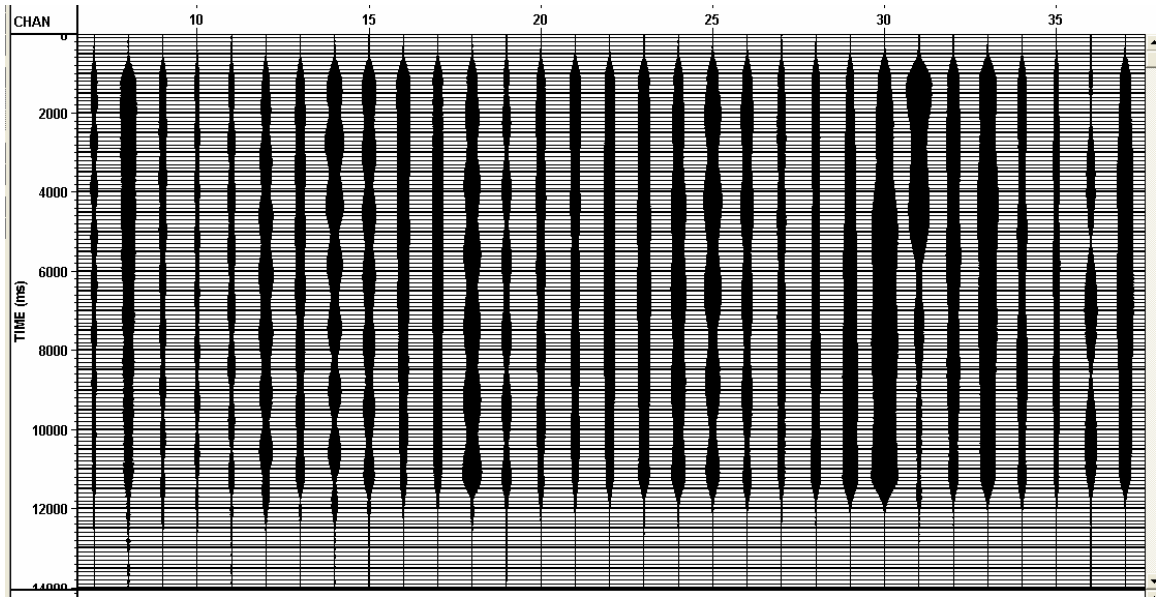
CHAN
10
15
20
25
30
35
TIME (ms)
2000
4000
6000
8000
10000
12000

(c)

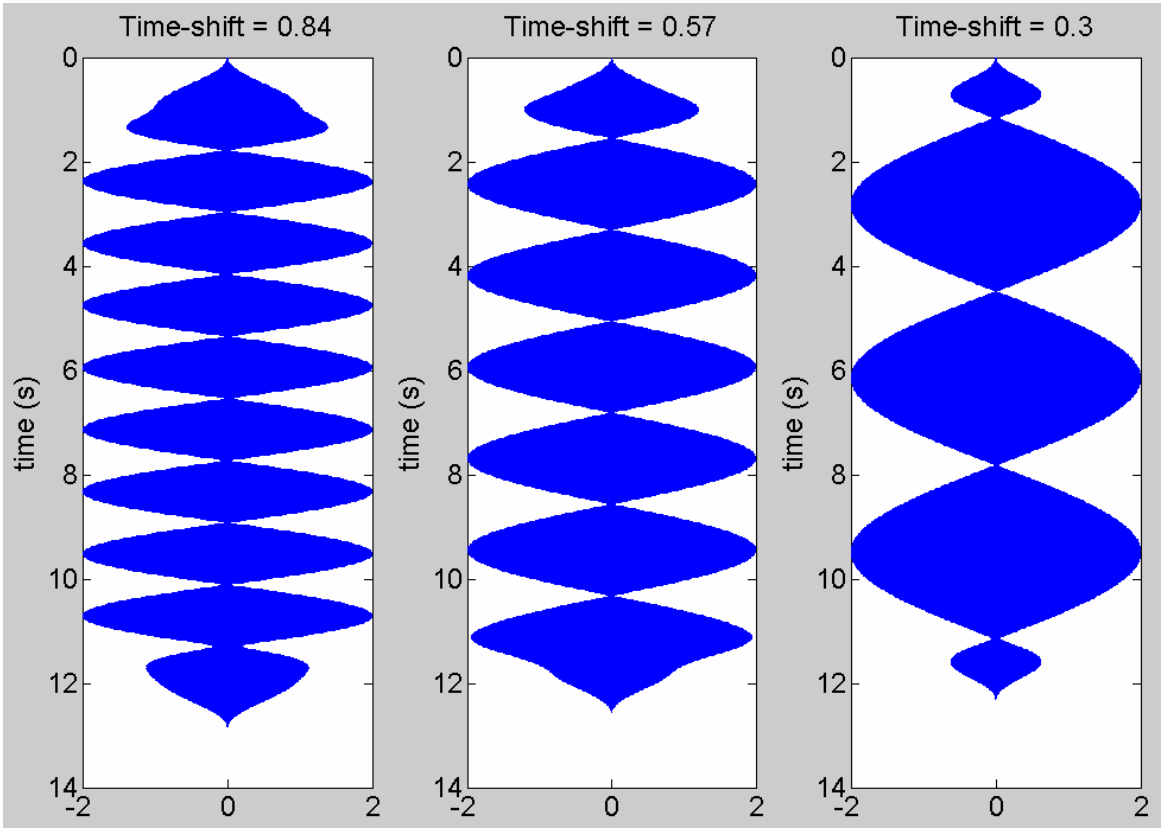

FIG. 7. (a) Mid-frequency traces. (b) Filtered mid-frequency traces. (c) Superpositions of mid-frequency sweep with time-shifted copies of itself.

(a)

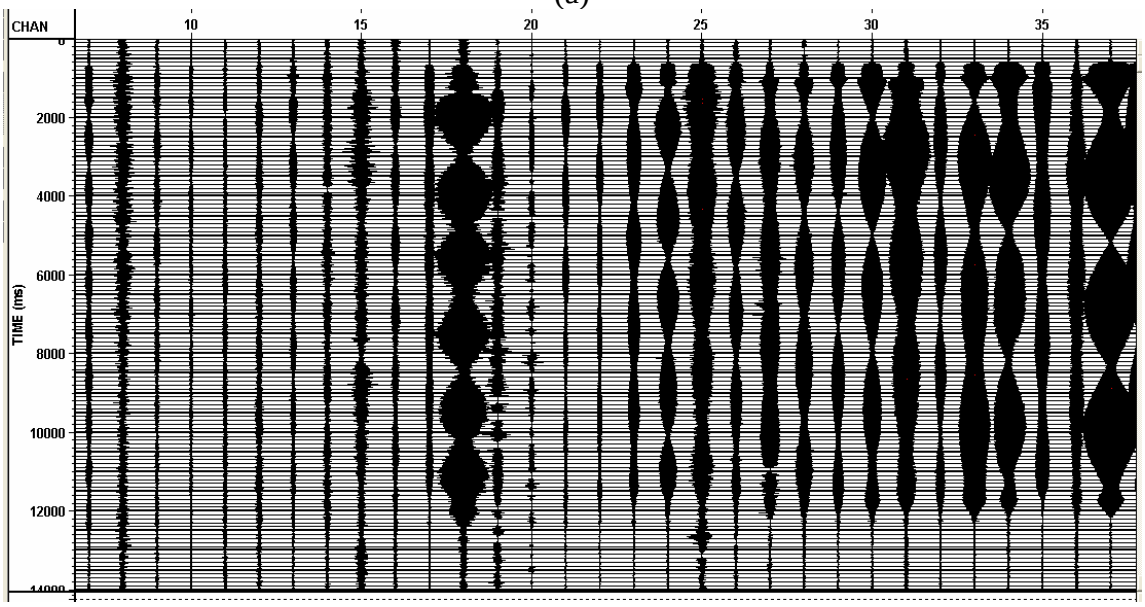

(b)

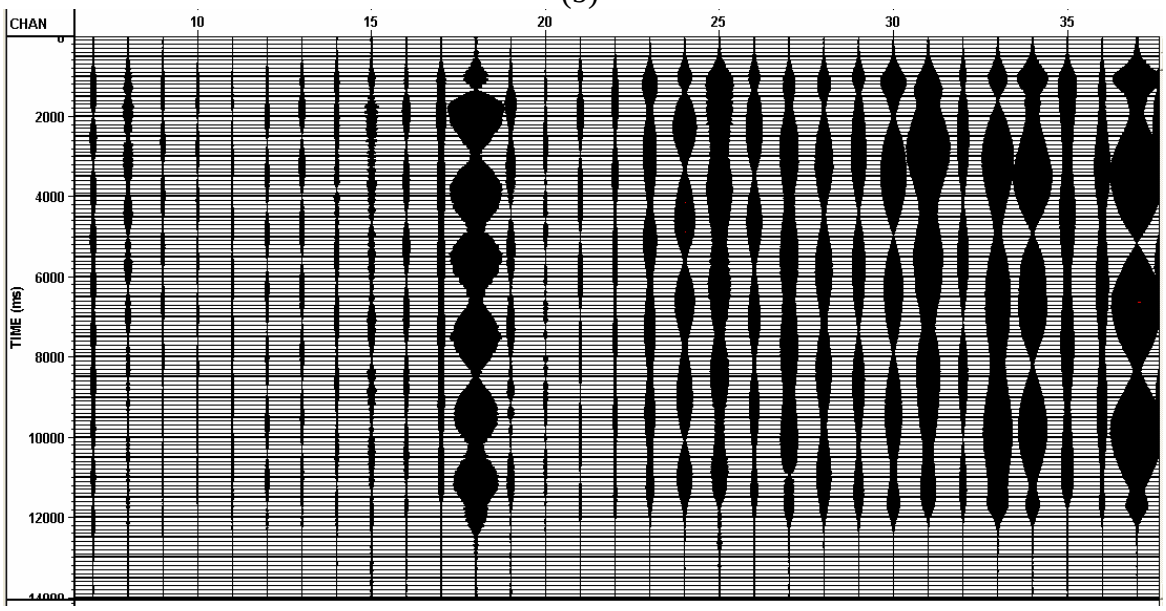

(c)

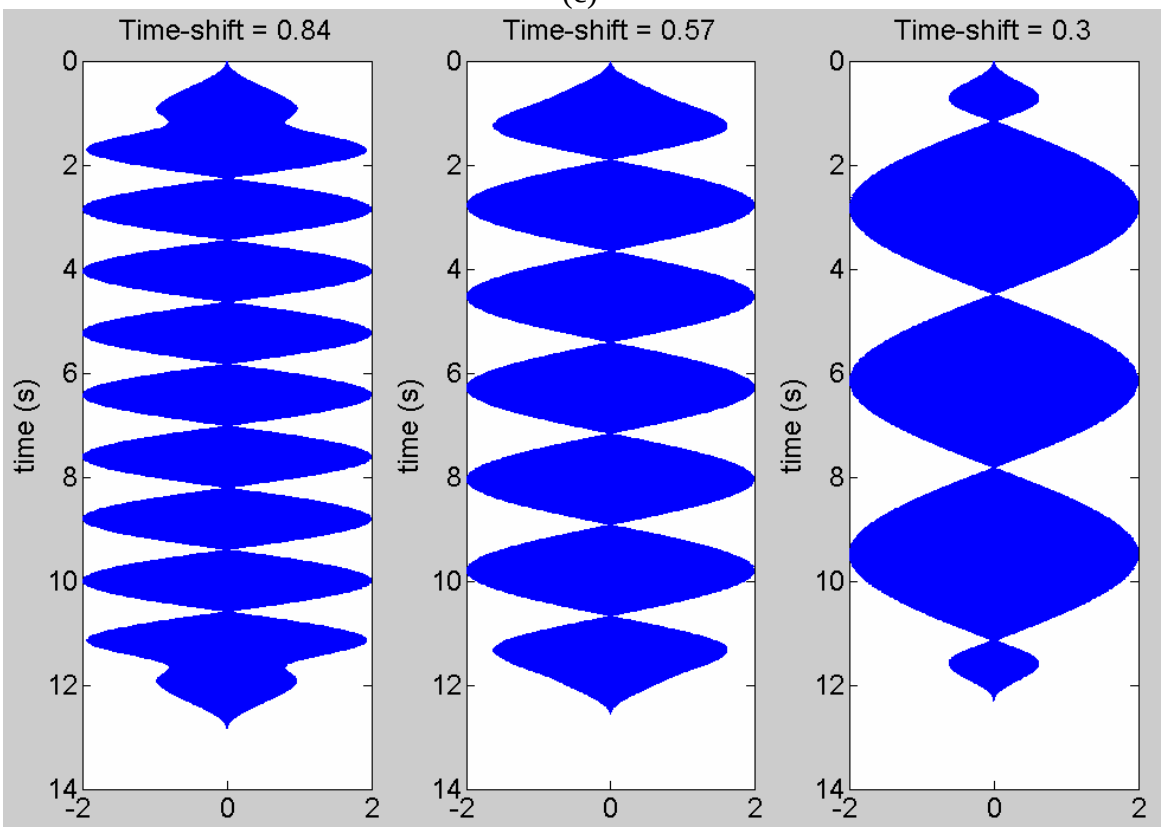

FIG. 8. (a) High-frequency traces. (b) Filtered high-frequency traces. (c) Superpositions of high-frequency sweep with time-shifted copies of itself.

BROAD-BAND SHOT RECORD DECOMPOSED INTO NARROW BANDS

Next we compare the true narrow-band signals with the broad-band signal filtered into the same frequency ranges. Ormsby filters were constructed analogously to the narrow-band sweep designs (e.g. 14/15-25/26 Hz filter for the low-frequency range).

Figures 9-11 display the results of low-, mid- and high-frequency bandpass filtering applied to the broad-band correlated shot record, and may be compared with Figures 2-4. Differences with filtered versions of Figures 2-4 are also displayed. These were obtained by using a least-squares procedure to obtain a scalar S which minimizes the quantity

$$\sum_{i,j}\left(u^{NB}(i,j) - Su^{BB}(i,j)\right)^2, \qquad (1)$$

where $u^{NB}(i,j)$ and $u^{BB}(i,j)$ are narrow-band and broad-band shot records, both with the same narrow-band filter applied, and i and j are indices representing trace number and time sample. The quantity $u^{NB}(i,j) - Su^{BB}(i,j)$ is displayed in Figures 9b, 10b and 11b.

The band-limited broad-band shot records are very similar in appearance to the corresponding narrow-band records. The difference displays show that the similarity is greatest at low frequency, where the residual signal is similar in magnitude to the noise, whereas the residual signal is noticeably greater than the noise in the mid- and high-frequency difference displays.

(a)

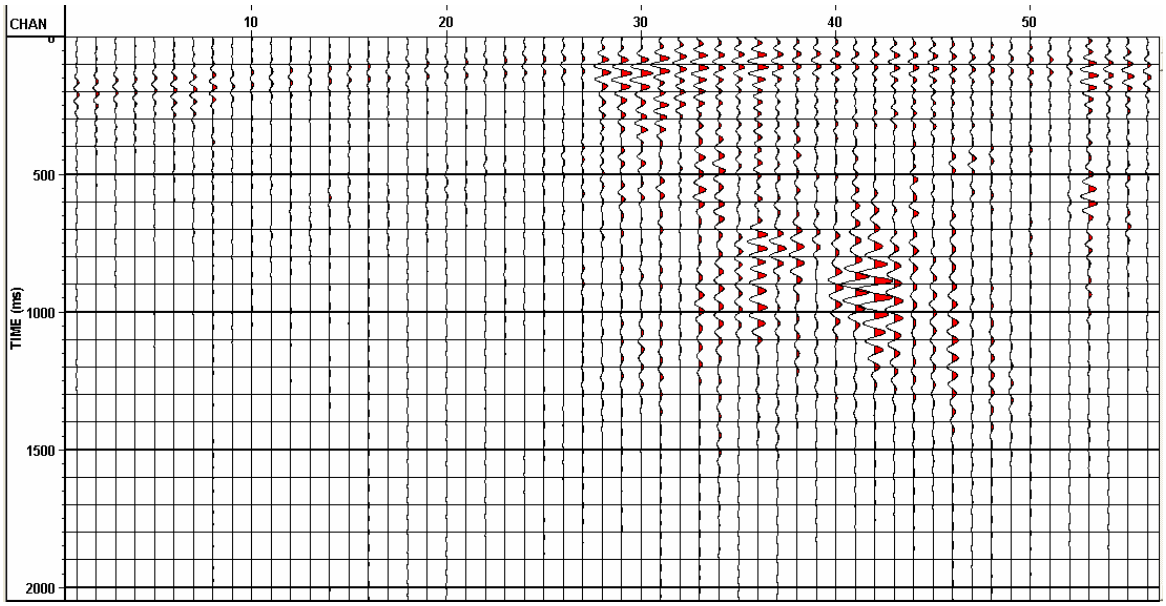

(b)

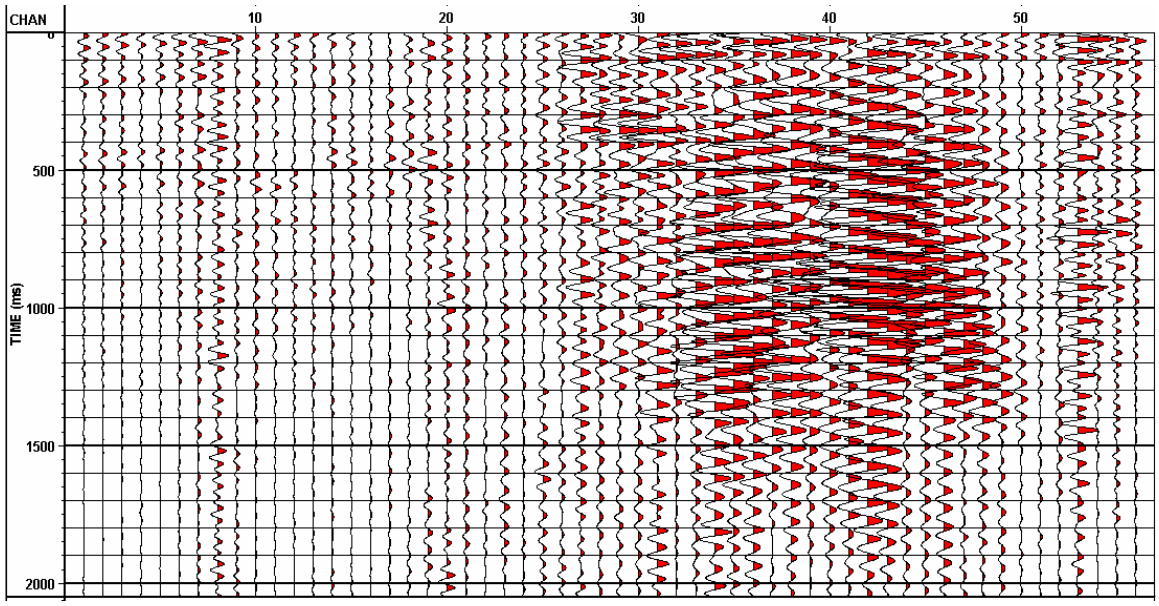

FIG. 9. (a) Low-frequency bandpass filter (14/15-25/26 Hz) applied to broad-band shot record. Compare to Figure 2. (b) Difference of Figures 2 and 9a (after best-fit scaling described in text). The final result in (b) has an overall scaling factor for visibility.

(a)

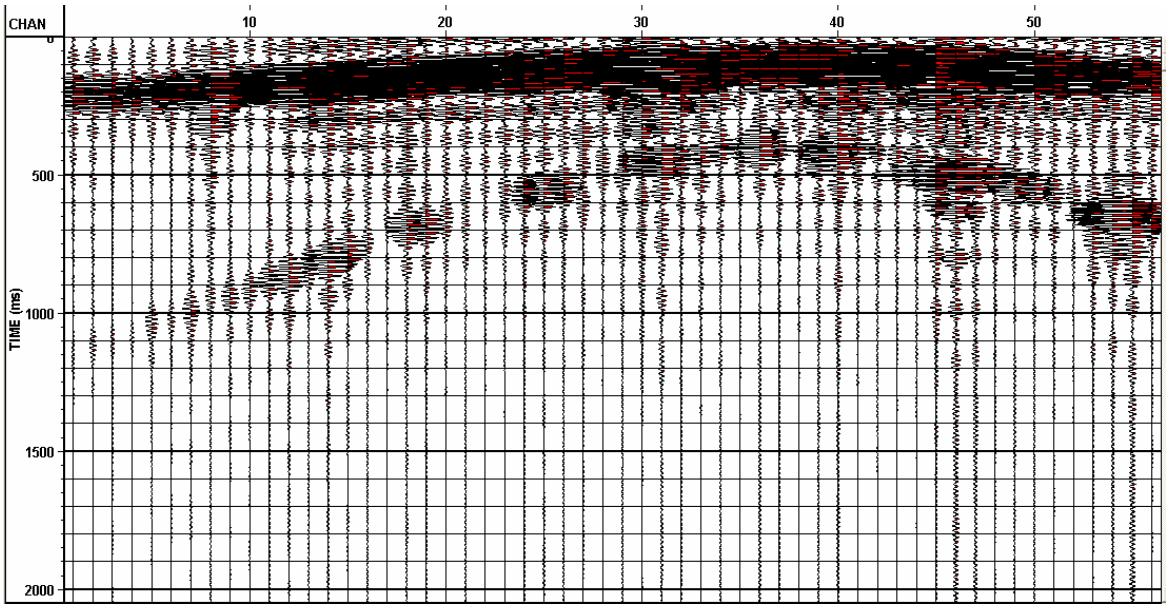

(b)

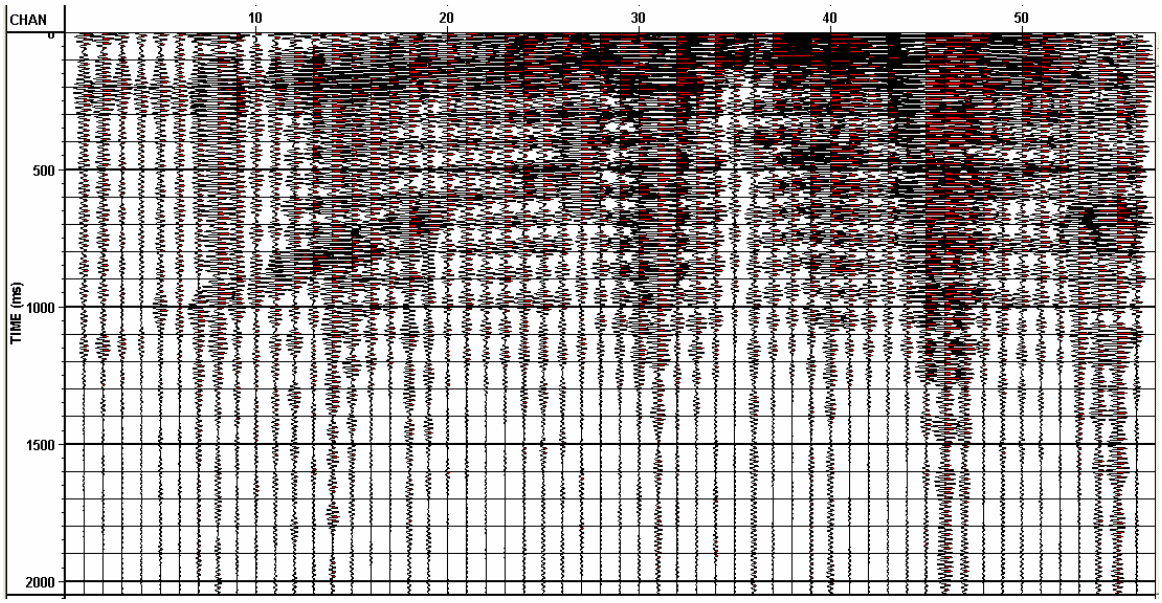

FIG. 10. (a) Mid-frequency bandpass filter (54/55-65/66 Hz) applied to broad-band shot record. Compare to Figure 3. (b) Difference of Figures 3 and 10a (after best-fit scaling described in text).

(a)

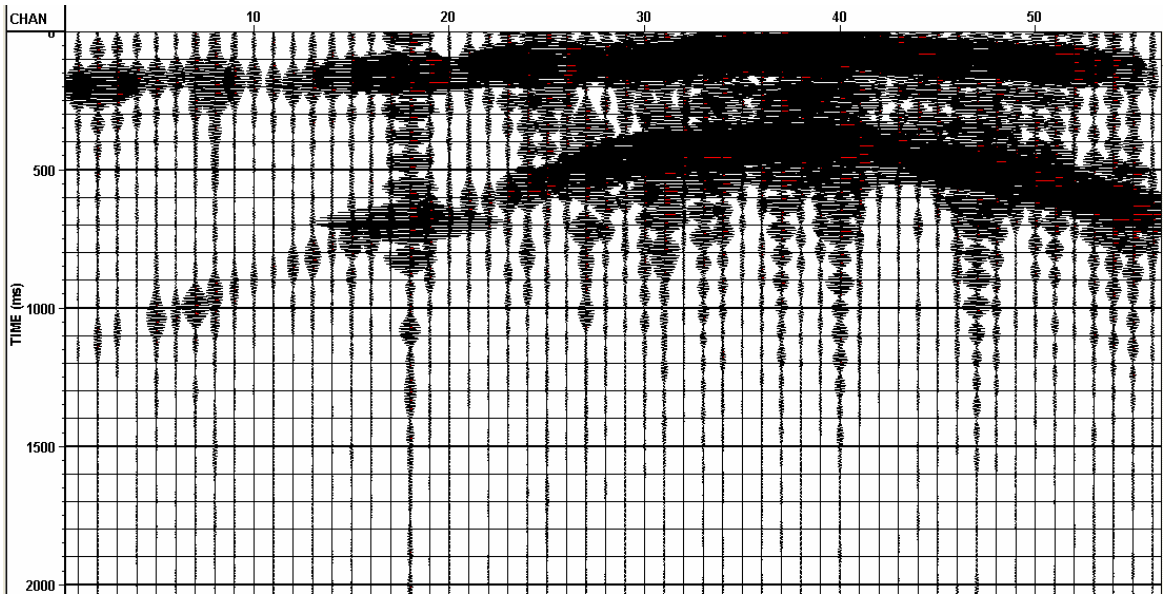

(b)

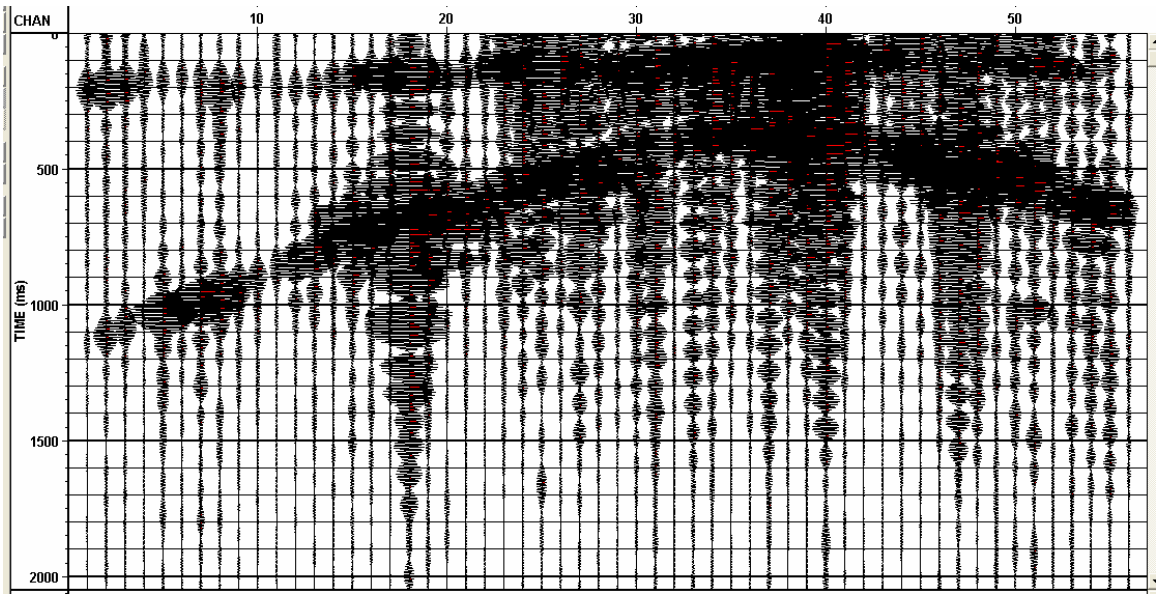

FIG. 11. (a) High-frequency bandpass filter (94/95-105/16 Hz) applied to broad-band shot record. Compare to Figure 4. (b) Difference of Figures 4 and 11a (after best-fit scaling described in text).

The values of *S* calculated from the minimization of equation 1 give some idea of the signal power of each shot record. For the low-, mid-, and high-frequency cases, *S* is equal to 8.869, 9.281, and 8.921 respectively. These are all in the vicinity of the ratio of bandwidths for the broad-band and narrow-band cases, i.e. 110 Hz / 12 Hz = 9.17. Thus the broad-band sweep spends about 1/9 as much time in each narrow frequency band as is spent in that same band during a narrow frequency sweep. Figure 12 displays both the narrow-band and scaled broad-band versions of trace #15, filtered into the narrow band,

along with their difference. These show that differences are greater for high-frequency traces.

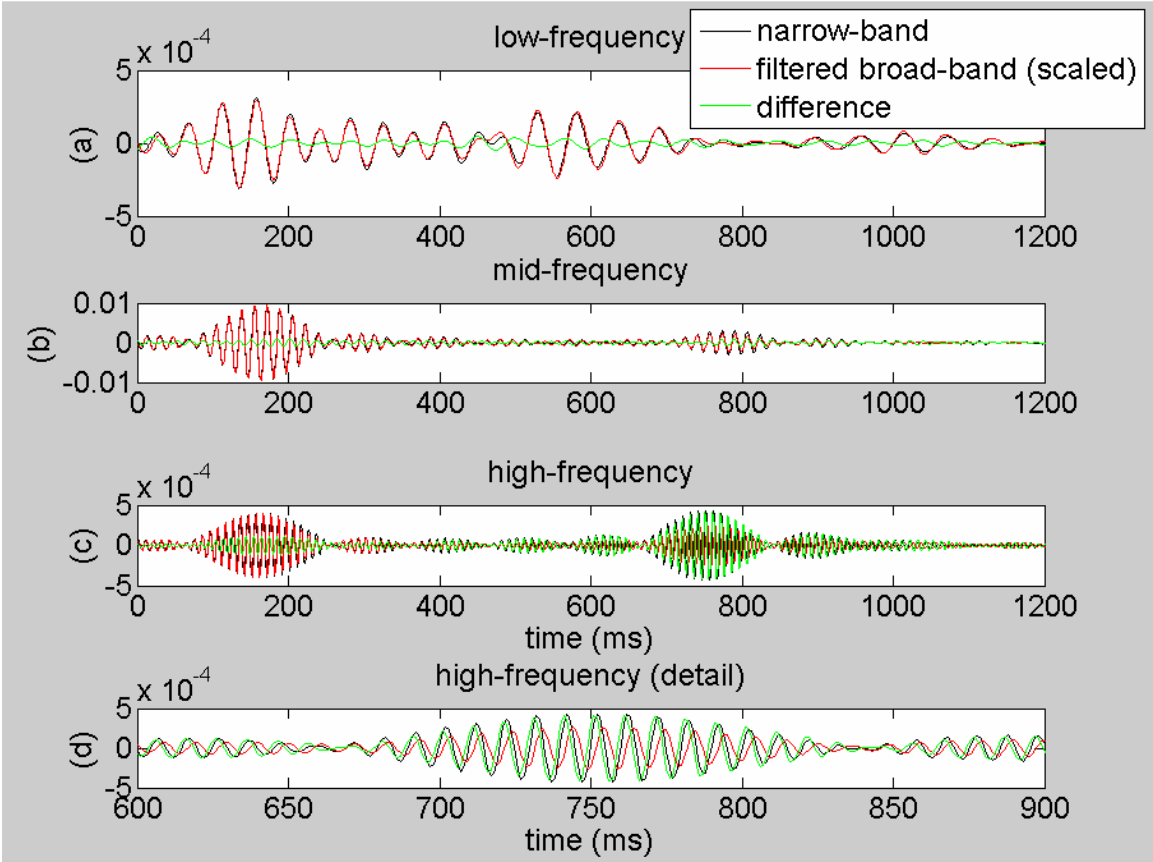

Figure 12. Narrow-band and scaled broad-band versions of trace #15, along with their difference for the (a) low-frequency, (b) mid-frequency, and (c) high-frequency cases. For clarity, one region of the high-frequency case is shown in detail in (d). Differences are most significant in the high-frequency case.

NARROW-BAND SHOT RECORDS COMPOSED INTO BROAD-BAND STACK

In this section we add together all nine narrow-band shot records and compare the result with Figure 1, the broad-band shot record. Figure 13a shows the result of adding together the raw shot records. Figure 13b shows the result of adding after first applying a narrow bandpass filter to each shot record to remove out-of-band noise. The two results are very similar to each other. They are also similar in many respects to Figure 1. The events are more sharply defined than in the individual narrow-band shot records. The main difference between Figure 1 and Figure 13 is that the lobe structure of the narrow-band Klauder wavelets is evident in Figure 13. This somewhat obscures the reflection event at 300 ms. The presence of sidelobes would appear to be the principal challenge in reproducing a broad-band shot record from several narrow-band records. It would be of interest to see if more carefully constructed Gaussian bands are more successful in reproducing a broad-band result.

(a)

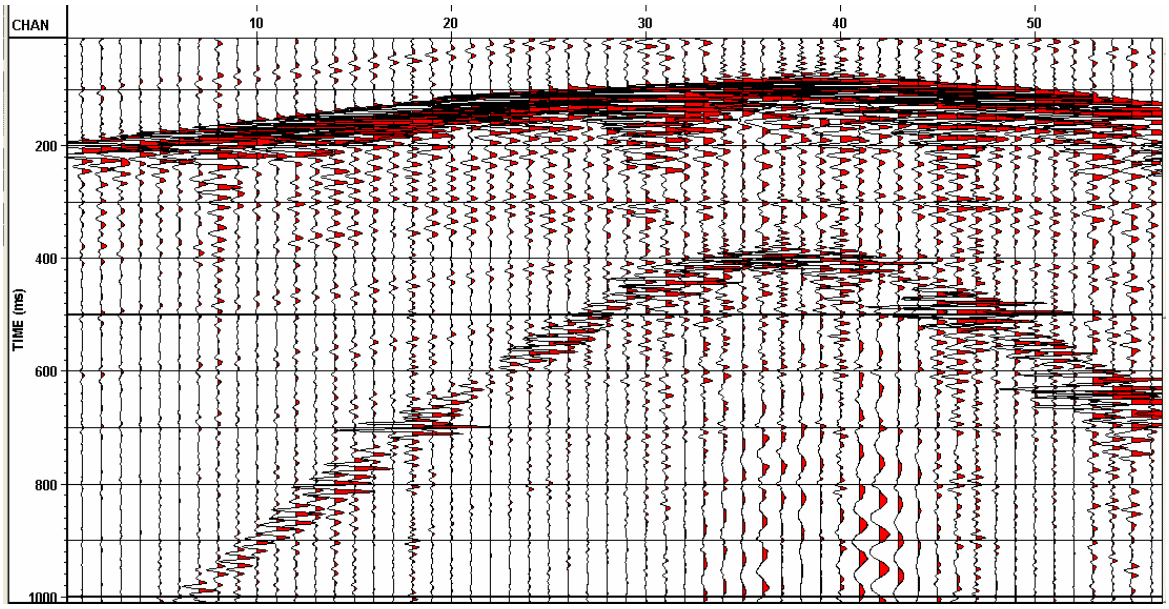

(b)

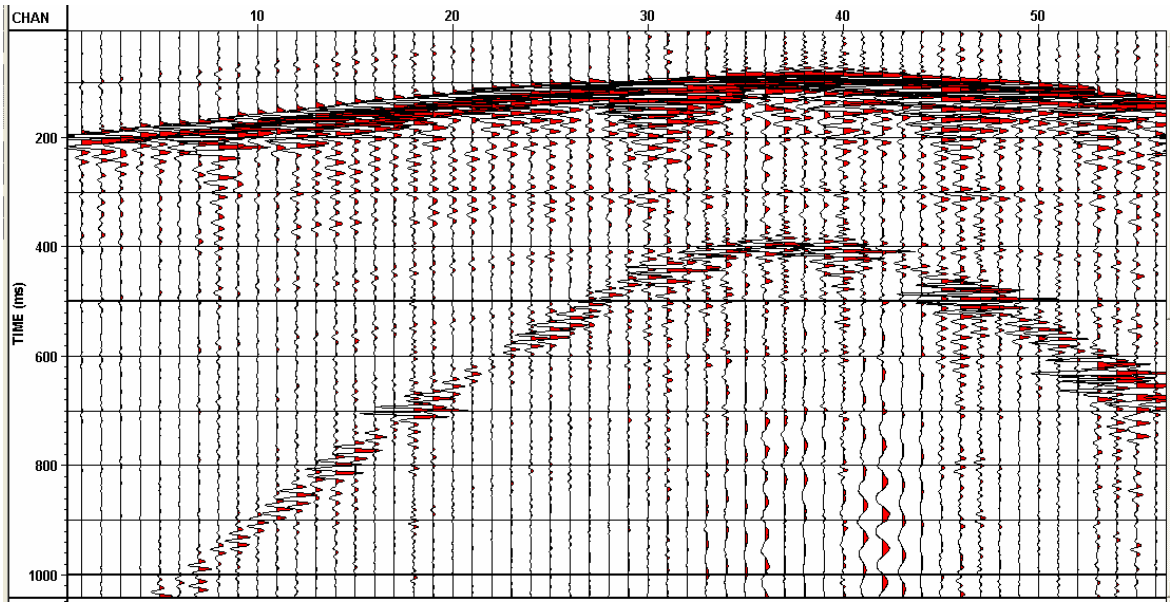

Figure 13. Sum of all nine narrow-band shot records (cf. Figure 1). (a) The raw shot records have been summed. (b) Out-of-band noise has been removed from the narrow-band shot records prior to summing. Narrow-band Klauder wavelet sidelobes are apparent in both (a) and (b), obscuring the reflection event at 300 ms.

BROAD-BAND TRACES DECOMPOSED INTO NARROW BANDS

In contrast to the decomposition of correlated shot records, we find that applying a narrow bandpass filter to a broad-band uncorrelated trace produces a signal with much less resemblance to the true narrow-band traces. This may be seen by comparing Figures 14-16 to Figure 6-8. Theoretically this can be explained using the convolution theorem.

According to this the spectrum of an uncorrelated trace is $W(f)R(f)$, and that of the correlated trace is $|W(f)|^2 R(f)$, where $W(f)$ is the spectrum of the sweep and $R(f)$ is the spectrum of the earth's reflectivity. Thus the phase of the correlated trace is the phase of the reflectivity, while the phase of the uncorrelated traces is a combination of sweep and reflectivity phases. If W_B is a broad-band sweep, and W_N is a narrow-band sweep, then it is straightforward to design a zero-phase filter, $F(f)$, such that $F(f)|W_B(f)|^2 R(f) \approx |W_N(f)|^2 R(f)$. However, applying $F(f)$ to the uncorrelated trace $W_B(f)R(f)$ may give it an amplitude similar to $W_N(f)R(f)$, but will leave its phase unchanged. Thus the sequence of events in time is not necessarily similar between the two resulting narrow-band traces. This corresponds to the intuitively obvious fact that each narrow frequency band is compressed into a much smaller time window in the broad-band sweep than in the narrow-band sweeps.

It is of interest however that if we extract out an appropriate time window for each filtered result, as shown in Figures 14b, 15b and 16b, then an improved comparison emerges nonetheless. This is particularly evident for the mid- and high-frequency cases, where the variation in envelope nodes varies with trace sequence number in a manner similar to that seen in Figures 7b and 8b.

We note that trace-by-trace RMS scaling has been applied, as average amplitude in these windows increases strongly from left to right.

(a)

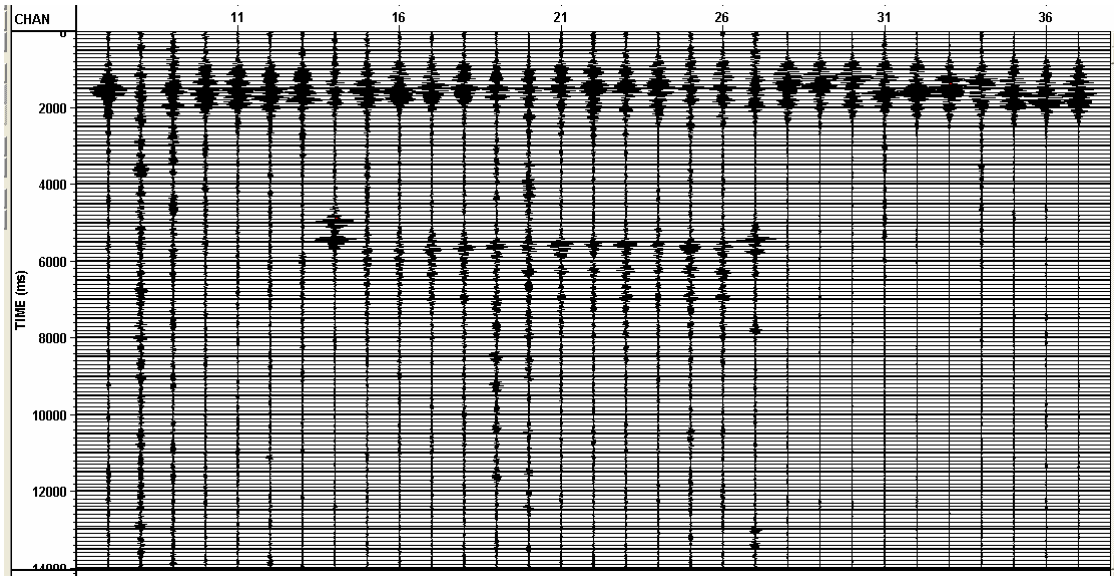

(b)

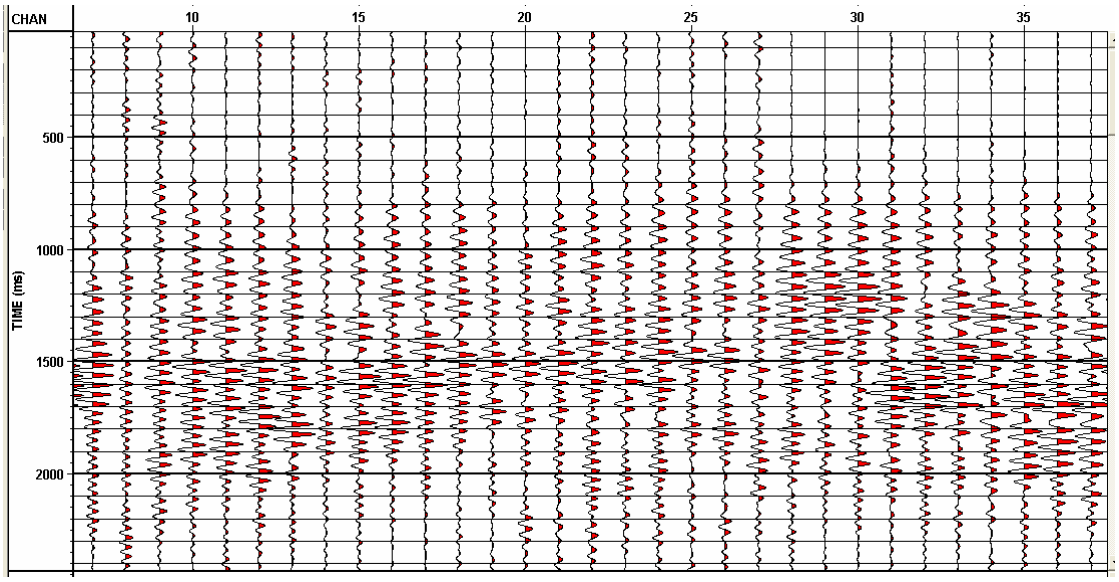

FIG. 14. Low-frequency bandpass filter (14/15-25/26 Hz) applied to broad-band uncorrelated traces. (a) Full 12 second traces. (b) Detail of window from 0 to 2.5 seconds. Compare to Figure 6.

(a)

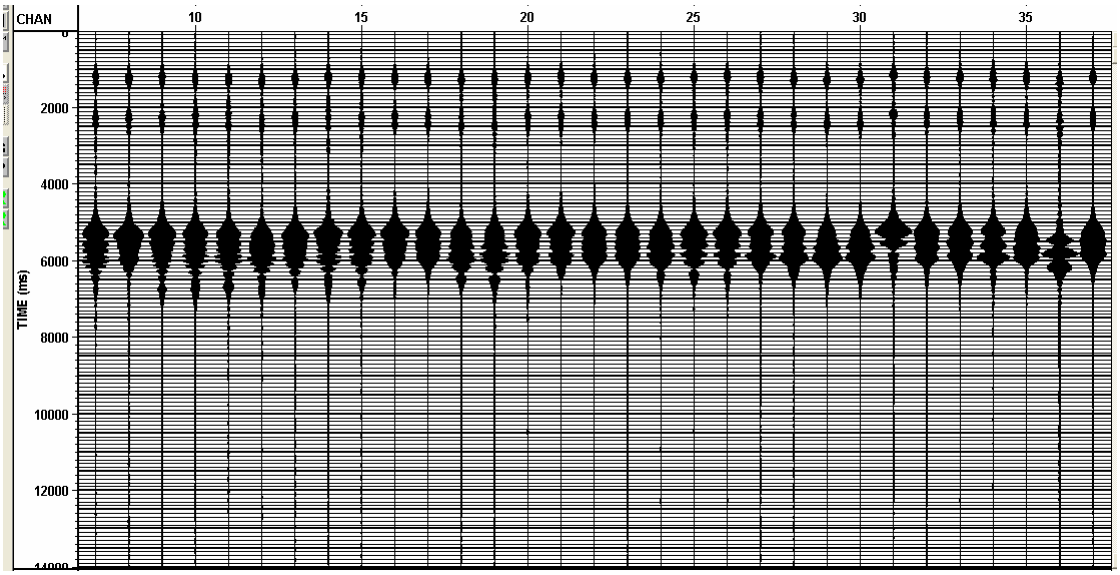

(b)

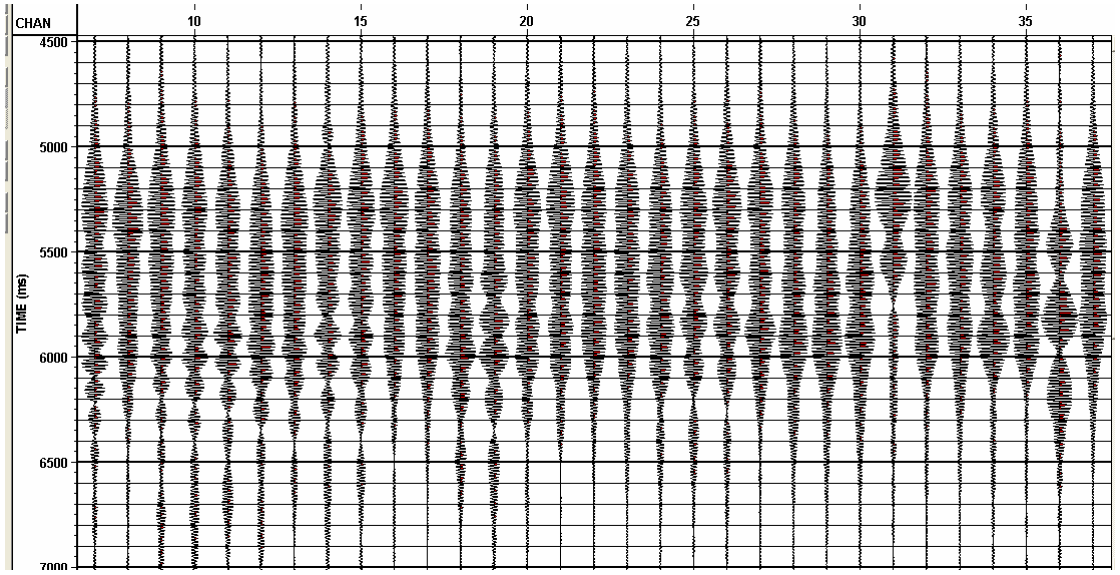

FIG. 15. Mid-frequency bandpass filter (54/55-65/66 Hz) applied to broad-band uncorrelated traces. (a) Full 12 second traces. (b) Detail of window from 4 to 7 seconds. Compare to Figure 7.

(a)

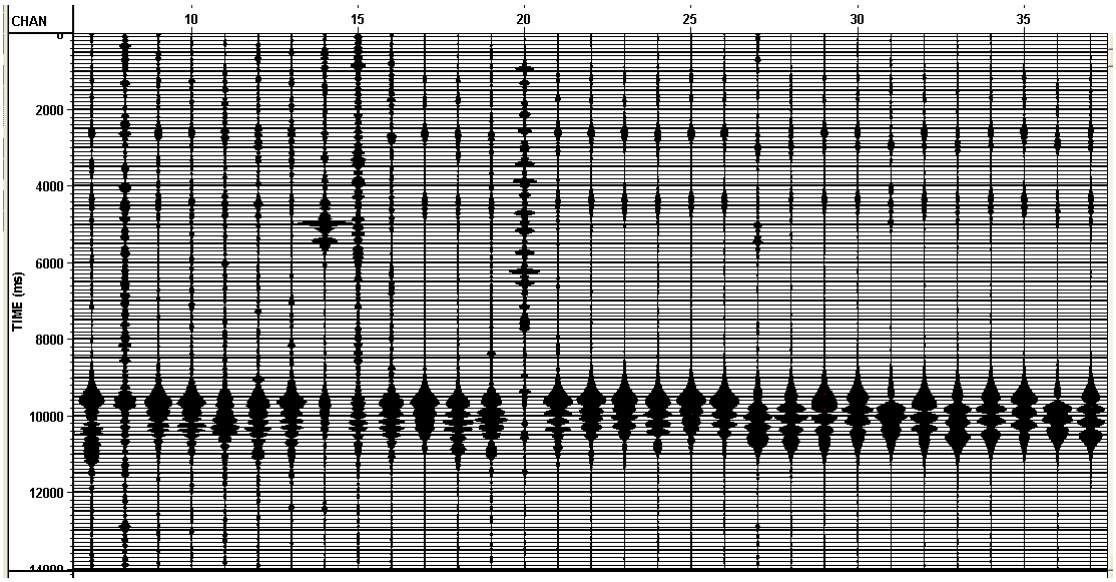

(b)

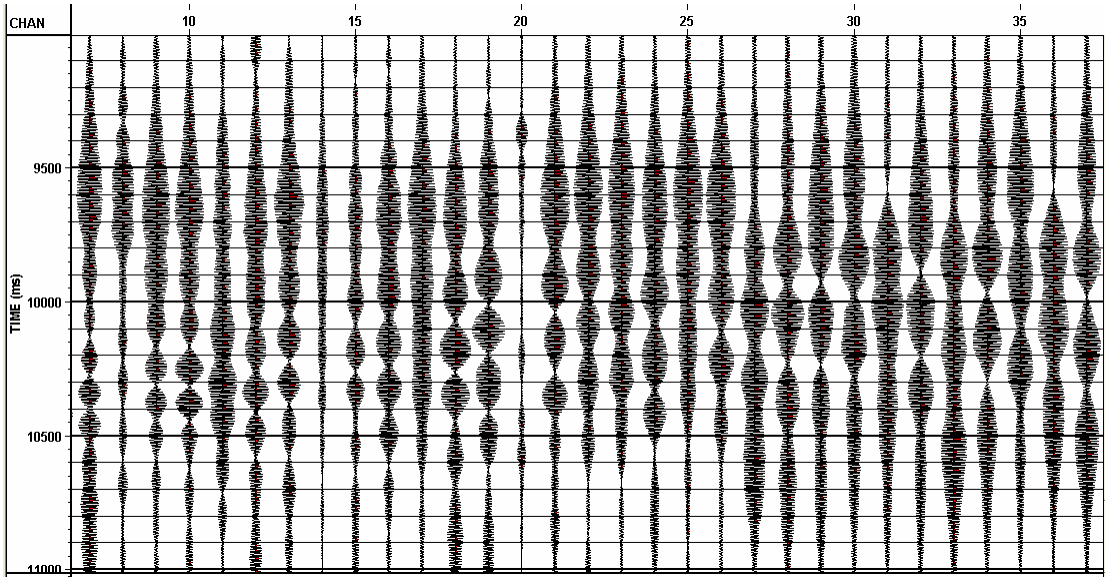

FIG. 16. High-frequency bandpass filter (94/95-105/16 Hz) applied to broad-band uncorrelated traces. (a) Full 12 second traces. (b) Detail of window from 9 to 11 seconds. Compare to Figure 8.

Trace reproducibility

It may be asked if the above comparisons are unreliable because of variations between repeated sweeps. To address this question, two separate narrow-band, mid-frequency traces are displayed together in Figure 17, along with their difference. From this figure it appears that, as far as the issues discussed in this report are concerned, repeated sweeps are essentially identical.

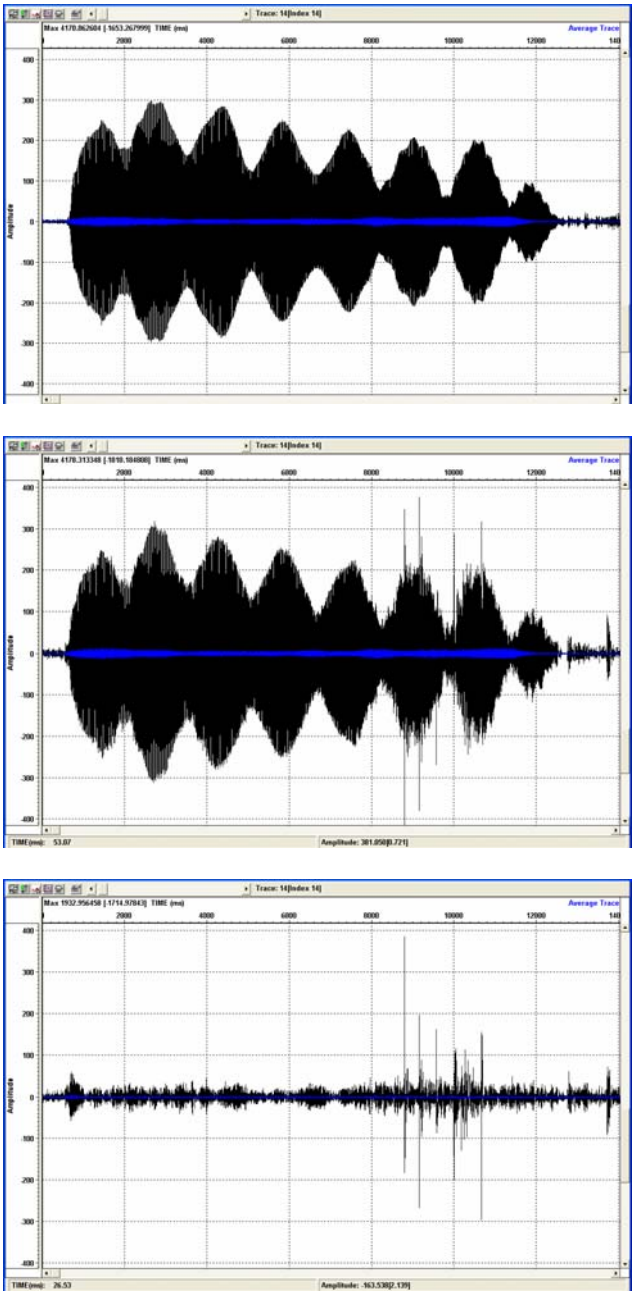

FIG. 17. Two mid-frequency traces, and their difference. The first display is trace #14 in Figure 7a. The second is a repeated sweep with the same parameters. Both have been RMS scaled to the same overall amplitude. The third display is of the difference, displayed on the same scale.

KLAUDER WAVELETS OF TAPERED SWEEPS

We now revisit the Klauder wavelets displayed earlier in this report. Figure 18a displays the Klauder wavelet shown in Figure 1b, but with an expanded time scale for comparison with narrow-band wavelets. Figure 18b, shows a wavelet similar to that displayed in Figure 3b, but with the band modified slightly to 54.5 – 65.5 Hz, instead of 54 – 66 Hz. The reason for this is that, with a 1 s taper, bandwidths centered at 10 Hz intervals will add together to give a constant power across their overlaps. In Figure 18c,

we present a wavelet for a new band, 50 – 70 Hz with a 10 s taper. This is defined so that the two tapers meet at 60 Hz to form a very smooth band, and frequency bands of this type centered at 10 Hz intervals will again add together to give a constant power across their regions of overlap. This band is designed as a simple approximation to the Gaussian band discussed earlier. Figure 18 shows that it retains approximately the same resolution as the previously defined narrow-band wavelet, but does not suffer from a train of large side lobes. This suggests that it would indeed be worthwhile to reacquire this data with smoothly shaped band functions.

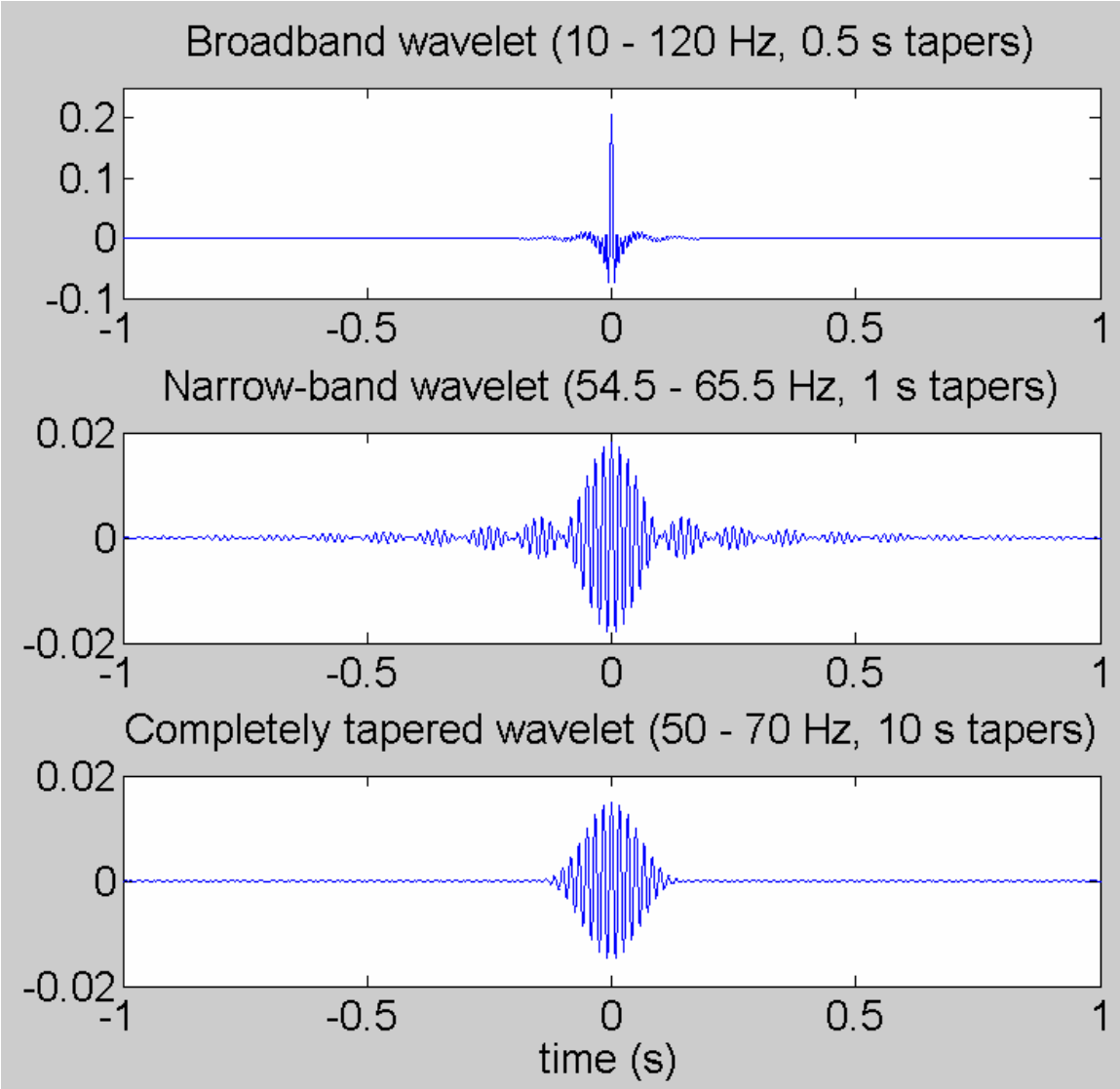

Figure 18. Klauder wavelets for (a) a typical broad-band seismic sweep (cf. Figure 1b), (b) a mid-frequency narrow-band sweep, similar to that discussed earlier in this report (cf. Figure 3b), and (c) a narrow-band sweep with tapers meeting smoothly in the centre of the band. Note that the ringing side lobes of (b) are absent in (c), while the resolution remains approximately the same.

CONCLUDING REMARKS

In a novel exercise, vibrator equipment owned by the Department of Geoscience at the University of Calgary has been employed to collect a polychromatic data set composed of several narrow-band sets of data. This has been collected both as separate, uncorrelated traces, as well as in the form of stacked, correlated data. This data is a deliverable we can provide to any of our sponsors interested in working with such data.

A preliminary assessment has shown the data to have reasonable features. We have also shown that, a broad-band correlated shot record may be reasonably decomposed into narrow-band components, particularly for the lower frequencies. The individual narrow-band components can conversely be composed into a pseudo-broad-band correlated shot record. The main obstacle in this exercise is the presence of side lobes that persist into the result. We have demonstrated that this may be alleviated by using narrow bands with smoother features.

In contrast to correlated records, a broad-band uncorrelated trace cannot in general be reliably decomposed into narrow-band traces. However, the small time window related to the narrow frequency band when expanded has a similar appearance to the original narrow-band traces, especially at high frequencies. Thus perhaps a very long broad-band trace, whose duration equals the sum of the narrow-band sweep times, could be reliably decomposed into narrow-band traces. It would be of interest to demonstrate this in a future acquisition.

Our primary future interests in this area are to repeat this survey with true Gaussian narrow bands, as well to explore other modes of polychromatic data collection, and to use such data in the development of techniques for *Q*-estimation from surface seismic.

ACKNOWLEDGEMENTS

We wish to acknowledge the generous donation of VISTA software by GEDCO, and the support of CREWES sponsors.

REFERENCES

Ursenbach, C. P., Bancroft, J. C., Bertram, M. B., Bland, H. C., Haase, A. B., Lawton, D. C., Margrave, G. F. , and Stewart, R. R., 2006, Proposal for a polychromatic seismic survey, CREWES Research Report, **18**.

Lu, H.-X., Hall, K. W., Henley, D. C., and Lawton, D. C., 2007, Processing report for the Alder Flats 3D, June 2007, CREWES Research Report, **19**.

Margrave, G. F., 2007, CREWES MATLAB Toolbox: www.crewes.org.